Journal Pre-proof

Visual clarity methylammonium lead trichloride perovskite single crystals for X and gamma rays protection

Qiang Xu, Wenyi Shao, Yang Li, Hang Zhang, Xiao Ouyang, Xinlei Zhang, Jing Nie, Xiaoping Ouyang, Bo Liu

PII: S0925-8388(19)33135-4

DOI: https://doi.org/10.1016/j.jallcom.2019.151896

Reference: JALCOM 151896

To appear in: *Journal of Alloys and Compounds*

Received Date: 24 June 2019

Revised Date: 12 August 2019

Accepted Date: 15 August 2019

Please cite this article as: Q. Xu, W. Shao, Y. Li, H. Zhang, X. Ouyang, X. Zhang, J. Nie, X. Ouyang, B. Liu, Visual clarity methylammonium lead trichloride perovskite single crystals for X and gamma rays protection, *Journal of Alloys and Compounds* (2019), doi: https://doi.org/10.1016/j.jallcom.2019.151896.

Graphical Abstract

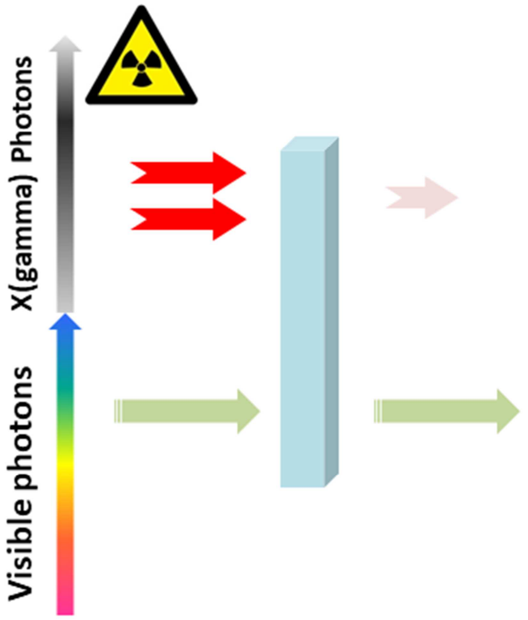

Visual clarity methylammonium lead trichloride perovskite single crystals for X and Gamma rays protection

Qiang Xu, [a,*] Wenyi Shao, [a] Yang Li, [a] Hang Zhang, [a] Xiao Ouyang, [b] Xinlei Zhang, [a] Jing Nie, [a] Xiaoping Ouyang, [a,b,c] and Bo Liu [d]

[a]Department of Nuclear Science and Engineering, Nanjing University of Aeronautics and Astronautics, Nanjing 211106, China

[b]College of Physics, Institute of Nuclear and New Energy Technology, Tsinghua University, Beijing, 100084. Beijing, China

[c] Northwest Institute of Nuclear Technology, Xi'an, 710024, China

[d]School of Physics Science and Engineering, Tongji University, Shanghai 200092, China

*Corresponding author: xuqiangxmu@nuaa.edu.cn (Q.X)

ABSTRACT

Ionization radiation photons such as X-ray and gamma ray have been widely applied in the nuclear power industry, medical imaging, scientific research, and aerospace exploration. Developing a protective material with excellent shielding properties and clear visibility is an urgent demand in order to protect people who are working in a radiation environment. Hence, we present a highly efficient radiation shielding material based on lead halide organic-inorganic perovskite single crystals with visual clarity, high efficiency and attenuation coefficient, and thin half-value layer. Our results indicate that the shielding performances (mass attenuation coefficients, effective atomic numbers and half value layer) of the perovskite crystals are at least one order higher than the current commercial products, such as Bone-equivalent plastic, Polyethylene terephthalate, and colorless glass. In addition, properties, physical properties (density), and optical properties (transmission, refractive index), can be slightly tuned by the dopant Br concentration in crystals. The present results demonstrate that the organic-inorganic perovksite single crystals are optimized for high attenuation radiation shielding materials with visual clarity.

Keywords: Perovskite single crystals, Radiation shielding, X-ray protection, Gamma-ray protection, High attenuation coefficient

1. Introduction

Radiation photons (X-ray or gamma ray) have been employed as valuable tools in medical, agriculture, scientific research, homeland security and aerospace exploration [1-6]. While all these applications are greatly helpful for human life, unwanted exposures such as scattering X-rays, emergency accidents and cosmic ray are hazardous to lives with varying effects. High dose radiation can produce immediate harmful effects, such as skin burn, radiation sickness, and radiation can increase the risk of cancer [7,8]. Therefore, how to prevent radiation that could cause physical harm to human and their surroundings is a serious safety concern to use that equipment, which potentially emits hazardous rays [9,10].

The incident photons either scattered or absorbed in a single event through various interaction process with atoms, electrons or nuclei of materials [11]. Thus, high atomic number (Z) materials have been employed to attenuate the X-ray or gamma ray. In general, metallic shielding materials with a high density such as iron (Fe), lead (Pb), tungsten (W) are effective alternatives for reducing the intensity of radiation. Among those heavy metallic materials, Pb is traditionally the most popularly and widely material used for providing durable shielding of gamma rays and X-rays, due to its high atomic number and easy process. However, these heavy and bulky metallic materials could not serve all the requirements of most applications [12]. For example, mobile nuclear devices and manned space crafts, lightweight and have less volume radiation shielding materials are preferred due to space and maneuverability constraints imposed by the vehicles. In addition, in medical and scientific research, optically clear with full radiation protection is suitable for observation windows to protect observers, operators, or workers [13].

Recently, numerous research focuses on lead-based shielding materials with transparent in visible light for shielding the unwanted X or gamma radiation. Lead glass and polymer are the most successful commercial products for X(γ) ray shield. Lead glass is heavy, expensive and easily breakable, the density of the polymer is low and with weak attenuation performance. In addition, the shielding efficiency of those materials is lower than the theoretical expectation, especially when they are thin [14]. Therefore, there are still some challenges that limit their applications such as cost, weight and optical properties (refractive index, nonlinear optical susceptibility, infrared transparency) [15]. Much efforts still seek to develop new shielding materials with low cost, high attenuation coefficients, the visible light transparent and other specific physical properties that can reduce as much as possible harmful X or gamma rays to meet the particular safety requirement [10-15]. A visual clarity shielding material is expected to have high transparent, high attenuation coefficients and thin half value layer that can significantly attenuate the incident radiation intensity with relatively small materials.

Organic-inorganic methylammonium lead halide perovskite materials $CH_3NH_3PbX_3$ ($MAPbX_3$, where MA is CH_3NH_3, X=Br, I, Cl) have been attracted in a variety of optoelectronics applications such as solar cell, light emitting diodes (LEDs), laser and photodetectors [16-19]. The outstanding performances of these applications are mainly attributed to the electronic properties (high mobility–lifetime product, long diffusion length and low trap density) and optical properties (high absorption coefficient, tunable direct optical band-gap) [20-22]. In addition, thanks to the existence of heavy atoms enhanced the ionization radiation attenuation properties, perovskite also has been successfully demonstrated to detect ionization radiation (charged particles, X(γ) ray) [23-26]. Therefore, perovksite materials are optimal for radiation shielding.

In this paper, we have successfully grown a high quality visible light transparent

$MAPbBr_xCl_{3-x}$ SCs with various dopant concentration and thickness by using the solution growth method. These organic-inorganic perovskite materials exhibit high transparent and attenuation coefficients with high effective radiation shielding performance. The shielding performance for 59keV photons is more than 10 times higher than that of polymer composites [27-29].

2. Experimental section

2.1 Synthesis of perovskite single crystals

Synthesis of perovskite single crystals: High quality perovskite single crystals were synthesized by using inverse temperature crystallization growth method with two steps. Firstly, growth CH_3NH_3Cl (MACl) powder using a molar ratio of 1:1 methylamine (33 wt% in absolute ethanol) and hydrochloride acid (33 wt% in water) stirred at 0℃ ice bath for 1.5 h. To increase the purity, the raw, as-grown MACl powder was washed with ethanol and diethyl ether for at least three times, until it appears snow white. Then, prepare precursor solution by dissolving various molar ratios of MACl, $PbBr_2$ (99.99%), $PbCl_2$ (99.99%) into 2 mol dimethyl sulfoxide (DMSO, 99%) until it saturated. A 2μm PTFE filter was used to filter the precursor solution, and then semi-transparent high-quality Br-doped $MAPbCl_3$ SCs were harvested from solution after increasing its temperature to 90 ℃. The size of the crystal was determined by the growth time.

2.3. Characterization

The element's content of crystals was characterized by a homemade X-ray fluorescence (XRF) spectroscopy system at room temperature. This system consists of X-ray tube, a silicon drift detector (Amptek XR-100SDD) with a Be window and a laser rangefinder. Optical transmission spectrum was recorded using a Cary 5000 UV-Visible spectrometer in the range of 350-600nm.

The radiation shielding performances were recorded by a radiation dosimeter and spectroscopy detection system. The pulse height spectrum was recorded by a High purity Germanium (HPGe) detector from ORTEC inc. X-ray photons were coming from X-ray tube (Mo target) operated at a various voltage, which collimated by a copper collimator with the diameter of 2mm. Am-241 (0.25μCi) and Pu-238 (8.79mCi) were employed as excited γ ray radiation source. To avoid the effect of emitted alpha particles from the Am-241 source, a thin layer of 0.5mm Teflon was covered on the radiation surface. All the measurements were in air at room temperature.

3. Results and discussion

3.1. Materials characterization

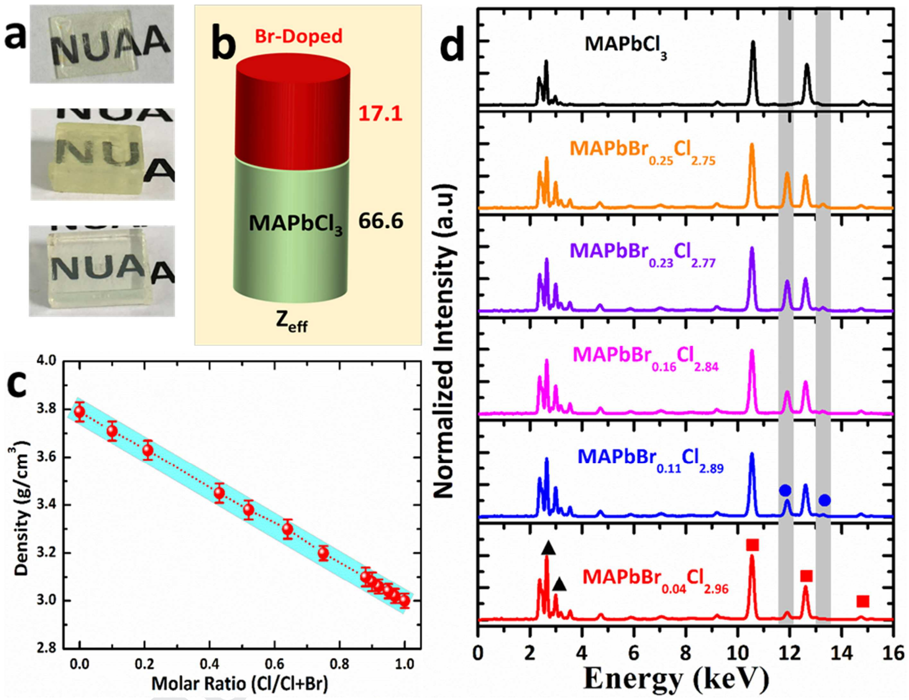

Fig. 1. Physical properties of $MAPbBr_xCl_{3-x}$ SCs. (a) side view of three $MAPbBr_xCl_{3-x}$ SCs with different thickness and Br dopant concentration. (b) calculated effective Z value of crystals with various Br content. (c) the density of $MAPbBr_xCl_{3-x}$ SCs as a function of Br concentration. (d) XRF spectra of $MAPbBr_xCl_{3-x}$ SCs that excited by 25keV X-ray from a portable X-ray tube with a silver anode, operated at 25kV. The black triangle stands for Cl element, the red square stands for Pb element, the blue circle stands for Br element. This measurement is carried in the air at room temperature, thus the signals from the air and background shielding materials have been recorded.

Various semi-transparent Br dopant $MAPbCl_3$ SCs with different thickness have been harvested from the saturated dimethyl sulfoxide (DMSO) solution (Materials and growth method) that consists of MACl, $PbCl_2$ and $PbBr_2$. The color of the crystals is determined by the Br concentration, the real optical images of $MAPbBr_xCl_{3-x}$ SCs as shown in Figure 1a. Effective atomic number (Z_{eff}) and density are two basic physical parameters that indicate the radiation shielding properties. High Z_{eff} and density are the two key strategies to obtain excellent shielding performance for X (γ) ray. Z_{eff} is theoretically given by using Mayneord's equation $Z_{eff} = \sqrt[2.94]{\sum_i n_i Z_i^n}$, where, n_i is the relative fraction of the total number of electrons, Z_i is the atomic number of each element [30]. The density of the crystals is measured from the real crystals. The Z_{eff} and density values are tuned from 66.6 and 3.0g/cm^3 to 83.7 and 3.79 g/cm^3 with the increasing of heavy atomic Br concentration (as shown in Figure 1b and 1c). To measure the Br concentration, we have investigated the crystals by using a homemade X-ray Fluorescence (XRF) analysis system [31]. Three main peaks ascribed to Pb, Cl and Br elements have been observed, the other peaks are from air and/or the background shielding materials. The actual molar ratio of Cl/(Cl+Br) in $MAPbBr_xCl_{3-x}$ SCs is obtained from these three peaks (Table 1).

Table 1 the chemical composition of $MAPbBr_xCl_{3-x}$

	Pb wt%	Cl wt%	Br wt%
$MAPbCl_3$	58.19	41.81	0
$MAPbBr_{0.04}Cl_{2.96}$	50.36	48.22	1.42
$MAPbBr_{0.11}Cl_{2.89}$	51.20	44.96	3.84
$MAPbBr_{0.16}Cl_{2.84}$	51.89	42.82	5.29
$MAPbBr_{0.23}Cl_{2.77}$	52.26	40.34	7.4
$MAPbBr_{0.25}Cl_{2.75}$	52.76	39.10	8.14

3.2 Optical properties

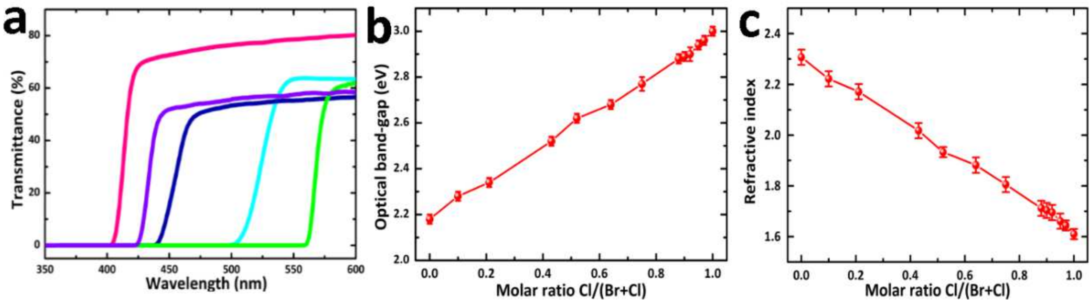

Fig. 2. Tunable optical properties of $MAPbBr_xCl_{3-x}$ SCs. (a) normalized transmission of $MAPbBr_xCl_{3-x}$ SCs in the range of 350 nm to 600 nm; (b, c) calculated optical band-gap and refractive index versus molar ratio of Cl/(Br+Cl).

Optical characterizations (transmission, optical band-gap and refractive index) of the $MAPbBr_xCl_{3-x}$ SCs are presented in Figure 2. Transmission spectra were carried out at room temperature by Cary 5000. The transmission of the crystals are depended by the thickness. Sharp and clear cut-off edges have been observed that tunable with the dopant Br content, which is attributed to band-gap absorption. Optical band-gap was extracted from the cut-off edge by using Tauc's equation. The relationship between optical band-gap and the molar ratio of Cl to Br+Cl is plotted in Figure 2b, that exhibits a nearly linear relationship with the increasing of Cl content from 2.18eV of $MAPbBr_3$ to 3.0 eV of $MAPbCl_3$. Refractive index is an important metric that determines the path of a visible photon at the interface at two media, and also correlates to the band-gap. The refractive index product is obtained using Moss equation: $E_g n^4 = k$, where k is a constant with a value of 108eV [32,33]. Figure 2c shows the calculated refractive index as a function of molar ratio, at a low content of Br, and the refractive index at around 2.3 has been obtained. With the increasing of Br content, refractive index is decreasing to about 1.6. The results indicate that the optical properties (transmission, optical band-gap and refractive index) of $MAPbBr_xCl_{3-x}$ SCs are strongly dependent by the concentration of dopant Br.

3.3 X- and Gamma rays shielding

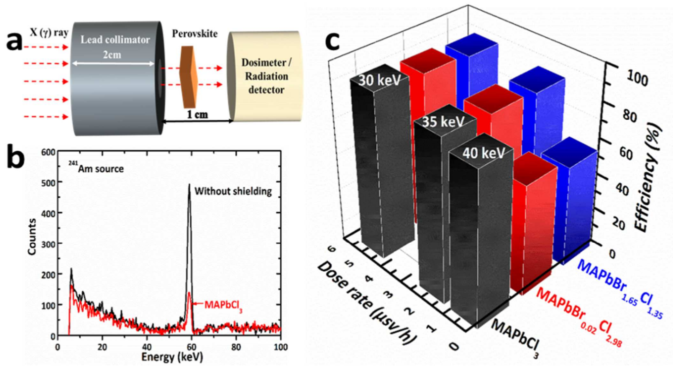

Fig. 3. Radiation shielding: (a) schematic of the experiment for radiation shielding measurement. (b) typical pulse height spectra distribution of γ ray that shielded by $MAPbCl_3$ SCs samples. The spectra were collected by High purity Germanium detector. The radiation source is Am-241 with the activity of 0.25 μCi. (c) radiation shielding efficiency of X-ray as a function of dopant Br and incident X-ray energy.

To measure the X(γ) ray shielding properties of the crystals, the schematic of our homemade measurement is shown in Figure 3a. It consists of a radiation source, lead collimator, and dosimeter or radiation detector. The radiation source of X-ray from an X-ray tube with Ag target and γ ray from radioactive isotope source, respectively. All radiation sources were collimated by a lead collimator with a diameter of 2mm. The shielding perovskite crystals were placed between collimator and detector with the same height. High purity Germanium (HPGe) detector and X(γ) ray dosimeter were employed to investigate the attenuation performance.

Figure 3b shows the pulse height spectra of Am-241 radiation source with and without shielding. To avoid the effect of the charged particles, a thin layer of white paper has been used to cover the surface of the source. When a thin $MAPbCl_3$ SCs with the dimension of 10.18mm (L)×11.2mm (W)×0.54mm (H) was employed to shield the 59keV γ-ray from the source, the intensity of photopeak is decreased several times. Furthermore, an X-ray tube with Mo target has been employed as a radiation source that operated at a different voltage. The dimension of the other two samples $MAPbBr_{0.02}Cl_{2.98}$ and $MAPbBr_{1.65}Cl_{1.35}$ are 9.6 mm (L)×9.7 mm (W)×0.49mm (H) and 10.43 mm (L)×11.55 mm (W)×0.35mm (H), respectively. These three samples presented good shielding efficiency, as shown in Figure.3c. The shielding efficiency is defined as $(1\text{-}I/I_0)\times100\%$, where, I is the initial radiation intensity, I_0 is the transmitted radiation intensity. The shielding efficiency is decreasing, while the energy of incident X-ray is increasing. The best shielding efficiency of these three samples is up to 90%, while the X-ray tube operated at 30kV.

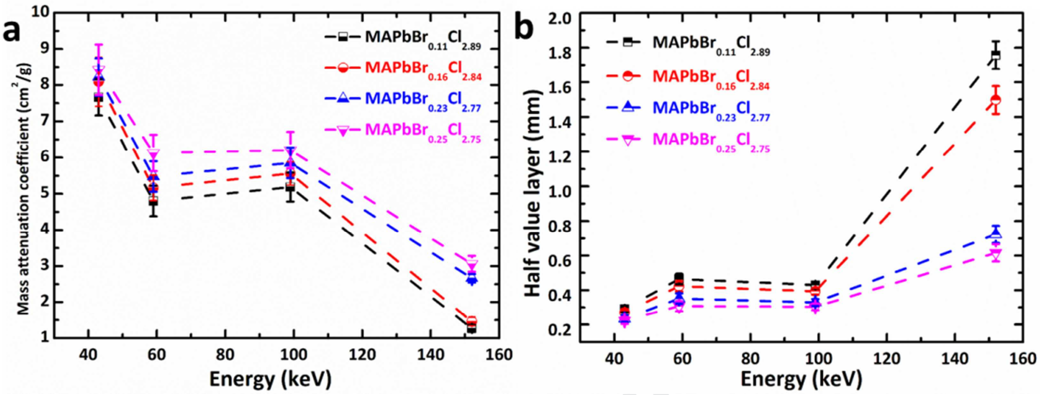

Fig. 4. (a) Mass attenuation coefficient and (b) half value layer of $MAPbCl_3$ with different dopant Br concentration, and as a function of photon energy.

It is worthwhile to be mentioned that the radiation shielding efficiency decreased with the Br doped into the perovskite SCs, this is ascribed to the different thickness of these three samples. Thus two precise metrics are used to evaluate the radiation shielding performance: mass attenuation coefficients ($^{\mu}/_{\rho}$) and half value layer (HVL). For a non-radiation scattering attenuation medium, according to Beer-Lambert's law equation, $I = I_0 e^{-(^{\mu}/_{\rho})\rho x}$, where $^{\mu}/_{\rho}$ is the mass attenuation coefficient, ρ is the density of material, I is the intensity of incident radiation photons and I_0 is the intensity of transparent radiation photons, and x is the thickness of the material. HVL is defined as the thickness of the materials at which the incident radiation intensity is reduced by one half. It is can be calculated from the equation of $HVL = {}^{0.693}/_{\mu}$.

To measure these two important metrics, a series of radioisotopes (Am-241: 59keV; Pu-238: 43keV, 99keV, 152keV;) have been used as gamma source. The values of $^{\mu}/_{\rho}$ and HVL for various Br dopant $MAPbCl_3$ SCs have been measured as shown in Figure 4. It is observed that the value of $^{\mu}/_{\rho}$ is increasing with the Br concentration, which is due to the higher density of crystals with more Br concentration than that of pure $MAPbCl_3$ single crystals. The ($^{\mu}/_{\rho}$) values are decreasing with the increasing of incident radiation photon energy, due to the weak attenuation efficiency. However, the values of ($^{\mu}/_{\rho}$) exhibit a weak increasing at 100keV comparing with 59keV, this is because of the X-ray absorption resonance at the electronic edge of Pb K shell in $MAPbBr_xCl_{3-x}$.

Table 2 Comparison of perovskite materials with comercial shielding materials at 59keV

Materials	Density (g/cm^3)	μ/ρ (cm^2/g)	HVL (cm)	(Z_{eff})	transparency	Ref
Bone-equivalent plastic (B-100)	1.45	0.253*	1.89*	7.57	clarity	**Error! Reference source not found.**[27]
Polyethylene terephthalate (mylar)	1.38	0.175*	2.87*	4.6	clarity	**Error! Reference source not found.**[27]
Al–steel composite foam	1.9-2.0	0.711	0.55	21.4	opacity	[28]
Aluminum A3 56	2.7	0.277	0.92	11.7	opacity	**Error**

						! Reference source not found.[28]
Steel–steel composite foam	2.7-2.8	0.92	0.28	26.8	opacity	[28]
Colourless glass	1.80-2.03	0.391-0.478	0.714-0.977	13.55-15.05	clarity	[29]
$MAPbBr_{0.25}Cl_{2.75}$	3.79	6.1	0.03	83.7	clarity	This paper

*Calculated result from the literature

We then compared the shielding performances of the perovskite materials with successful commercial products (polymer, plastic, glass). As shown in Tabel 2, our results indicate that the shielding ability of perovksite is about 10 times or more than Bone-equivalent plastic (B-100), Polyethylene terephthalate (mylar) [27], plastic [28], colourless glass [29].

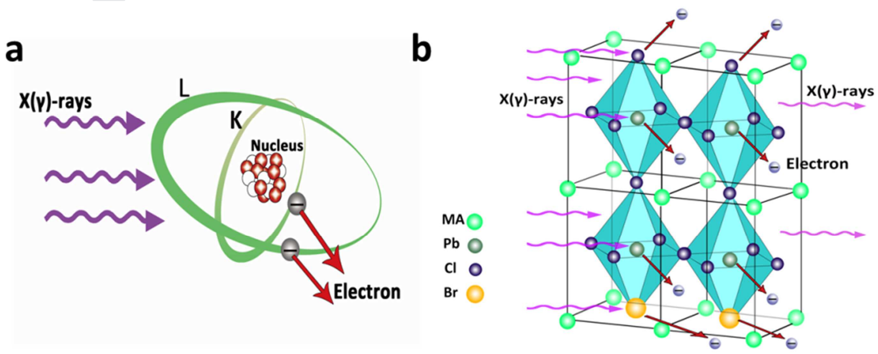

Fig. 5. Schematic of shielding process: (a) photoelectric effect process, electrons are emitted from atoms; (b) proposed mechanism of X (γ) interaction with $MAPbBr_xCl_{3-x}$ at low energy (<500keV). When a beam of X (γ) ray pass through the crystals and collides with heavy atoms (Pb, Br, Cl), it will transfer all of its energy to the eject

electron. Therefore, the incident X (γ) rays are attenuated by perovskite materials.

The shielding performances of perovskite materials are correlated to the interaction with incident ionization photons (X or γ ray). A beam of ionization photons exposure onto the materials, three main physical processes can occur while these photons interact with the materials: the photoelectric effect is the emission electrons from atoms; Compton scattering is the scattering of photons on electrons resulting energy loss; pair production is the absorbed photons created an electron-positron pairs near a nucleus. Thus, the total attenuation coefficients(μ_{total}) can be expressed as [34]:

$$\boldsymbol{\mu_{total} = \mu_{pe} + \mu_{comp} + \mu_{pair}} \qquad \textbf{(1)}$$

where, μ_{pe}, μ_{comp}, and μ_{pair} are the attenuation coefficients caused by photoelectric effect, Compton scattering, and pair production, respectively. For a given material, the interaction mechanism between photons and material are depended by incident photons energy. At low energy (<500keV), photoelectric absorption is the dominant process. As shown in Figure 5, the incident photon is completely absorbed by atomic and transfer its energy to the electron that ejected with a finite kinetic energy E_e:

$$\mathbf{E_e = E_\gamma - E_B} \qquad \textbf{(2)}$$

where, E_γ is the energy of the incident photon, E_B is the electronic binding energy [34,35]. However, not all the photons of the incident gamma ray could interact with perovskite (Figure 5b). The PE interaction cross-section is inversely proportional to gamma photon energy and atomic number, can be estimated as $\tau_{PE} \propto Z^n / E_\gamma^{3.5}$, where exponent n in the range of 4 to 5.

It is to be noticed that the slightly enhanced shielding performance of Br-doped materials is mainly caused by the K-shell of Br. The shielding performance (large value of (μ/ρ) and thin

HVL) at 100keV is better than at 60keV, this phenomenon is attributed to K-shell absorption edge of Pb [36].

3.4 Stability

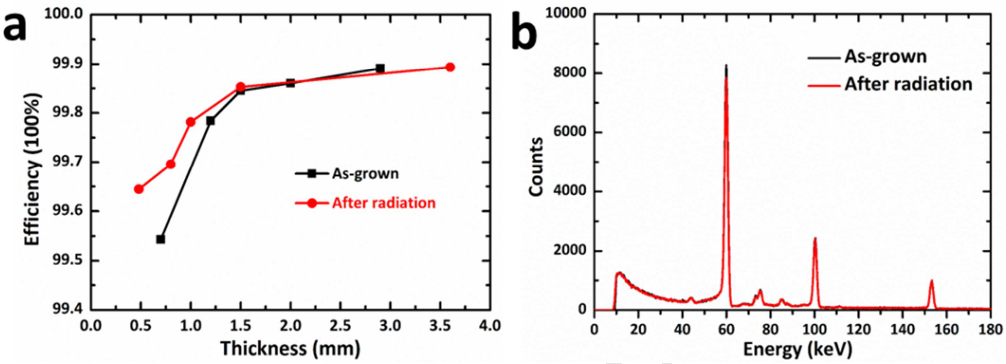

Fig. 6. Radiation stability: (a) intensity shielding efficiency of crystal, as grown and after radiation (b) comparison of pulse height spectra of Pu-238 radiation source after shielded by as-grown and after radiation $MAPbCl_3$ SCs crystals. The radiation gamma ray is from Co-60 source, after exposure for 8h with the dose rate of 5520Gy.

Radiation stability is another concerned problem for applications, therefore, we have evaluated the shielding stability of perovskite crystals under gamma ray. The crystals were loaded into the radiation room in Co-60 radiation center at Nanjing University of Aeronautics and Astronautics in the air at room temperature. The total exposure radiation dose rate is up to 5520Gy after 8h exposure. No significant degradation of shielding performance has been observed as shown in Figure 6a, b. The weak shielding efficiency degradation is mainly attributed to ion immigration under the photon irradiation, which is also demonstrated in previous literature [37,38].

4. **Conclusions**

High-quality $MAPbBr_xCl_{3-x}$ single crystals have been obtained by using a solution growth method at low temperature. The X(γ) photons radiation shielding properties (mass attenuation coefficients, effective atomic numbers, half value layer) of $MAPbBr_xCl_{3-x}$ SCs have been systematically investigated, and the radiation performances can be enhanced by the Br concentration. The perovskite crystals exhibited ultra-stability under a high dose rate of gamma ray irradiation. In addition, the crystals exhibit high transparency in the visible range with tunable cut-off edge and refractive index. These results indicate that the $MAPbBr_xCl_{3-x}$ SCs is optimal to provide radiation shielding that requires a visual clarity and radiation shielding applications, especially for medical treatment, imaging, diagnostic and industrial workplace.

Acknowledgements

This work was supported by the National Natural Science Foundation of China (11705090, 11875166, 11435010).

References

[1] A. Sakdinawat, D. Attwood, Nanoscale X-ray imaging, Nat. Photonics 4, (2010) 840-848.

[2] S. Kasap, J. B. Frey, G. Belev, O. Tousignant, H. Mani, J. Greenspan, L. Laperriere, O. Bubon, A. Reznik, G. DeCrescenzo, K. S. Karim, J. A. Rowlands, Amorphous and polycrystalline photoconductors for direct conversion flat panel X-ray image sensors Sensors 11 (2011) 5112-5157.

[3] J. A. Hernandez-Viezcas, H. Castillo-Michel, J. C. Andrews, M. Cotte, C. Rico, J. R. Peralta-Videa, Y. Ge, J. H. Priester, P. A. Holden, J. L. Gardea-Torresdey, In situ synchrotron X-ray fluorescence mapping and speciation of CeO2 and ZnO nanoparticles in soil cultivated soybean (Glycine max), ACS nano 7 (2013) 1415-1423.

[4] S. Cipiccia, M. R. Islam, B. Ersfeld, R. P. Shanks, E. Brunetti, G. Vieux, X. Yang, R. C. Issac, S. M. Wiggins, G. H. Welsh, M. P. Anania, D. Maneuski, R. Montgomery, G. Smith, M. Hoek, D. J. Hamilton, N. R. C. Lemos, D. Symes, P. P. Rajeev, V. O. Shea, J. M. Dias, D. A. Jaroszynski, Gamma-rays from harmonically resonant betatron oscillations in a plasma wake, Nat. Phys. 7, (2011) 867.

[5] K. Wells, D. A. Bradley, A review of X-ray explosives detection techniques for checked baggage, Appl. Radiat. Isotopes 70 (2012) 1729-1746.

[6] Fermi-LAT Collaboration, Gamma-ray emission concurrent with the nova in the symbiotic binary V407 Cygni, Science 329 (2010) 817-821.

[7] L. Mullenders, M. Atkinson, H. Paretzke, L. Sabatier, S. Bouffler, Assessing cancer risks of low-dose radiation, Nat. Rev. Cancer 9 (2009) 596-604.

[8] S. Grudzenski, A. Raths, S. Conrad, C. E. Rube, M. Löbrich, Inducible response required for repair of low-dose radiation damage in human fibroblasts, P. Natl. Acad. Sci. USA. 107 (2010) 14205-14210.

[9] S. Stathakis, The physics of radiation therapy, Med. Phys. 37 (2010) 1374-1375.

[10] O. Ciraj-Bjelac, M. M. Rehani, K. H. Sim, H. B. Liew, E. Vano, N. J. Kleiman, Risk for radiationKleiman, n, K. H. Sim, H. B. Liew, E. Vano, Ncardiology: Is there reason for concern? Catheter. Cardio. Inte. 76 826-834 (2010).

[11] J. E. Martin, Physics for radiation protection: a handbook, Physics for radiation protection: a handbook. (2006).

[12] E. J. Hall, A. J. Giaccia, Radiobiology for the Radiologist (Vol. 6). Philadelphia: Lippincott Williams & Wilkins, Radiobiology for the Radiologist. (2006).

[13] R. Fazel, H. M. Krumholz, Y. Wang, J. S. Ross, J. Chen, H. H. Ting, N. D. Shah, K. Nasir, A. J. Einstein, B. K. Nallamothu, Exposure to low-dose ionizing radiation from medical imaging procedures, New Eng. J. Med. 361 (2009) 849-857.

[14] J. P. McCaffrey, H. Shen, B. Downton, E. Mainegra-Hing, Radiation attenuation by lead and nonlead materials used in radiation shielding garments, Med. phys. 34 (2007) 530-537.

[15] S. Xu, M. Bourhamb, A. Rabieia, A novel ultra-light structure for radiation shielding, Mater. Design 31 (2010) 2140-2146.

[16] G. Maculan, A. D. Sheikh, A. L. Abdelhady, M. I. Saidaminov, M. A. Haque, B. Murali, E. Alarousu, O. F. Mohammed, T. Wu, O. M. Bakr, CH3NH3PbCl3 single crystals: inverse temperature crystallization and visible-blind uv-photodetector, J. Phys. Chem. Lett. 6 (2015) 3781-3786.

[17] B. He, W. Li, Q. Wang, L. Liang, H. Wang, J. Xu, S. Yang, Y. Jiang, Y. Tang, B. Zou, Ultrasensitive all-solution-processed field-effect transistor based perovskite photodetectors with sol-gel SiO2 as the dielectric layer, J. Alloys Compd. 717 (2017) 150-155

[18] B. R. Sutherland, E. H. Sargent, Perovskite photonic sources, Nat. Photonics 10 (2016) 295.

[19] B. Shen, Y. Wang, Z. Hu, S. Tang, Y. Chen, J.Zhang, Y. Zhu, Growth of monolithically grained CH3NH3PbI3 film by a uniform intermediate phase for high performance planar perovskite solar cells, J. Alloys Compd. 776 (2019) 250-258

[20] Q. Xu, W. Shao, X. Zhang, J. Liu, X. Ouyang, X. Tang, W. Jia, Low-temperature photoluminescence spectroscopy of CH3NH3PbBrxCl3-x perovskite single crystals, J. Alloys Compd. 792 (2019) 185-190.

[21] D. Shi, V. Adinolfi, R. Comin, M. Yuan, E. Alarousu, A. Buin, Y. Chen, S. Hoogland, A. Rothenberger, K. Katsiev, Y. Losovyj, X. Zhang, P. A. Dowben, O. F. Mohammed, E. H. Sargent, O. M. Bakr, Low trap-state density and long carrier diffusion in organolead trihalide perovskite single crystals, Science 347 (2015) 519-522.

[22] Z. Lian, Q. Yan, T. Gao, J. Ding, Q. Lv, C. Ning, Q. Li, J. L. Sun, Perovskite CH3NH3PbI3(Cl) single crystals: rapid solution growth, unparalleled crystalline quality, and low trap density toward 108 cm−3, J. Am. Chem. Soc. 138 (2018) 9409-9412.

[23] H. Wei, D. DeSantis, W. Wei, Y. Deng, D. Guo, T. J. Savenije, L. Cao, J. Huang, Dopant compensation in alloyed CH3NH3PbBr3−x Clx perovskite single crystals for gamma-ray spectroscopy, Nat. Materials 16 (2017) 826-833.

[24] Q. Xu, H. Wei, W. Wei, W. Chuirazzi, D. DeSantis, J. Huang, L. Cao, Detection of charged particles with a methylammonium lead tribromide perovskite single crystal, Nucl. Instrum. Meth. A 848 (2017) 106-108.

[25] W. Wei, Y. Zhang, Q. Xu, H. Wei, Y. Fang, Q. Wang, Y. Deng, T. Li, A. Gruverman, L. Cao, J. Huang, Monolithic integration of hybrid perovskite single crystals with heterogenous substrate for highly sensitive X-ray imaging, Nat. Photonics 11 (2017) 315-321.

[26] Q. Xu, W. Shao, Y. Li, X. Zhang, X. Ouyang, J. Liu, B. Liu, Z. Wu, X. Ouyang, X. Tang, W. Jia, High-Performance Surface Barrier X□ray Detector Based on Methylammonium Lead Tribromide Single Crystals, ACS Appl. Mater. Interfaces 11 (2019) 9679−9684.

[27] K. S. Mann, A. Rani, M. S. Heer, Shielding behaviors of some polymer and plastic materials for gamma-rays, Radiat. Phys. Chem. 106 (2015) 247-254.

[28] S. Chen, M. Bourham, A. Rabiei, Novel light-weight materials for shielding gamma ray. Radiat. Phys. Chem. 96 (2014) 27–37.

[29] S. Yasmin, Z. S. Rozaila, M. U. Khandaker, B. S. Barua, F. U. Z. Chowdhury, M. A. Rashid, D. A Bradley, The radiation shielding offered by the commercial glass installed in Bangladeshi dwellings, Radiat. Eff. Defect. S. 173 (2018) 657-672.

[30] W. V. Mayneord, Acta Int. Union Against Canc. 2 271-282 (1937).

[31] Q. Shan, X. Zhang, Y. Zhang, W. Jia,Y. Ling, D. Hei, S. Chu, Development of an online X-ray fluorescence analysis system for heavy metals measurement in cement raw meal, Spectrosc. Lett. 49 (2016) 188-193.

[32] T. S. Moss, Relations between the refractive index and energy gap of semiconductors, Phys. Stat. Sol. (B) 131 (1985) 415-427.

[33] T. S. Moss, A Relationship between the refractive index and the infra-red threshold of sensitivity for photoconductors, Pro. Phys. Soc. B. 63 (1950) 167.

[34] G. F. Knoll, Radiation Detection and Measurement. (2010).

[35] Q. Chen, J. Wu, X. Ou, B. Huang, J. Almutlaq, A. A. Zhumekenov, X. Guan, S. Han, L. Liang, Z. Yi, J. Li, X. Xie, Y. Wang, Y. Li, D. Fan, D. B. L. Teh, A. H. All, O. F. Mohammed, O. M. Bakr, T. Wu, M. Bettinelli, H. Yang, W. Huang, X. Liu, All-inorganic perovskite nanocrystal scintillators, Nature 561 (2018) 88.

[36] M. J. Berger, XCOM Photon Cross Sections Database; NIST Physics Laboratory: Gaithersburg, (1998).

[37] S. Yang, Z. Xu, S. Xue, P. Kandlakunta, L. Cao, J. Huang, Organohalide Lead Perovskites: More Stable than Glass under Gamma‐Ray Radiation, Adv. Mater. 31 (2018) 1805547.

[38] G. Y. Kim, A. Senocrate, T. Y. Yang, G. Gregori, M. Grätzel, J. Maier, Large tunable photoeffect on ion conduction in halide perovskites and implications for photodecomposition, Nat. Materials 17 (2018) 445.

1. The shielding performance for gamma ray (59keV) is more than 10 times higher than that of polymer composites.
2. The organic–inorganic perovskites exhibit high radiation stability under ^{60}Co gamma ray irradiation with dose rate up to 5520Gy after 8h exposure in air at room temperature.
3. The shielding performances and optical properties can be slightly tuned by halide Br doping concentration